



RESEARCH ARTICLE

10.1029/2018JA026321

Model of Jupiter's Current Sheet With a Piecewise Current Density

Key Points:

- A new model of Jupiter's current disk is developed and optimized to magnetic field data from Juno Perijove-01
- The model current varies inversely with radius in the ranges 7-30 and 50-95 R_J but inversely as the radius squared at radii between
- Compared with previous models similarly optimized, the new model shows the lowest RMS deviation

Correspondence to:

I. A. Pensionerov,
pensionerov@gmail.com

Citation:

Pensionerov, I. A., Alexeev, I. I., Belenkaya, E. S., Connerney, J. E. P., & Cowley, S. W. H. (2019). Model of Jupiter's current sheet with a piecewise current density. *Journal of Geophysical Research: Space Physics*, 124. <https://doi.org/10.1029/2018JA026321>

Received 20 NOV 2018

Accepted 25 FEB 2019

Accepted article online 28 FEB 2019

I. A. Pensionerov¹ , I. I. Alexeev¹ , E. S. Belenkaya¹, J. E. P. Connerney^{2,3} , and S. W. H. Cowley⁴

¹Federal State Budget Educational Institution of Higher Education M.V. Lomonosov, Skobeltsyn Institute of Nuclear Physics (SINP MSU), Moscow State University, Moscow, Russian, ²Space Research Corporation, Annapolis, MD, USA, ³NASA Goddard Spaceflight Center, Greenbelt, MD, USA, ⁴Department of Physics and Astronomy, University of Leicester, Leicester, UK

Abstract We develop a new empirical model of Jupiter's equatorial current sheet or magnetodisk, constructed by combining successful elements from several previous models. The new model employs a disk-like current of constant north-south thickness in which the current density is piecewise dependent on the distance ρ from Jupiter's dipole axis, proportional to ρ^{-1} at distances between ~ 7 and $\sim 30 R_J$ and again at distances between ~ 50 and $\sim 95 R_J$, and to be continuous in value but proportional to ρ^{-2} at distances between. For this reason we term the model the Piecewise Current Disk model. The model also takes into account the curvature of the magnetodisk with distance and azimuth due to finite radial propagation speed and solar wind effects. It is taken to be applicable in the radial distance range between ~ 5 and $\sim 60 R_J$. Optimized parameters have been determined for Juno magnetic field data obtained on Perijove-01, with the model showing overall the lowest root-mean-square deviation from the data compared with similarly optimized earlier models.

1. Introduction

The principal dynamics of the Jovian magnetosphere are governed by the strong planetary magnetic field, the fast rotation of the planet, and the presence of a large internal source of the plasma from the moon Io (Balogh, Beekand, et al., 1992; Balogh, Dougherty, et al., 1992; Bolton et al., 2015; Goertz, 1976b; Ness, Acuna, Lepping, Behannon, et al., 1979; Ness, Acuna, Lepping, Burlaga, et al. 1979; Ness, Acuna, Lepping, Burlaga, Behannon & Neubauer 1979; Smith et al., 1974, 1975; E. Smith, Connor, & Foster Smith et al., 1975; E. J. Smith, L. Davis, & Jones 1976). These features create azimuthal and radial currents in the equatorial plasma that result in the field lines becoming greatly distended away from the planet, forming a current sheet or magnetodisk configuration that is responsible for the Jovian magnetosphere's enormous size (Bagenal, 2007; Goertz & Ip, 1984; Hill, 1979; Vasyliunas, 1983). The distance from the center of the planet to the subsolar magnetopause can be more than $100 R_J$ (R_J is Jupiter's equatorial 1 bar radius 71,492 km; e.g., Joy, 2002).

Since Jupiter's current sheet was discovered, many models describing its structure have been created. The present work focuses on empirical modeling of the magnetodisk field, which will be considered in detail below. The other category of models is physical models that self-consistently include plasma properties and force balance. Caudal (1986) proposed a model which takes into account the centrifugal and pressure forces of the plasma, the pressure being taken to be isotropic. Nichols (2011) and Nichols et al. (2015) further improved this model, the latter paper, by including the effect of plasma pressure anisotropy.

Connerney et al. (1981) constructed an empirical model of Jupiter's current disk, which has formed the basis of many subsequent modeling studies. In this model the disk is assumed to carry only azimuthal currents; has a half thickness D , inner and outer radii of R_0 and R_1 , respectively; and is centered on the magnetic equator. The current density in the disk is distributed uniformly north-south across the width of the disk but is taken to be inversely proportional to the distance from the magnetic axis. As reviewed in section 2, these properties allow the model field to be written as exact integral expressions that may be evaluated numerically. Analytic approximations to the full solution have also been derived by Connerney et al. (1981) and Acuña et al. (1983), which have been augmented to divergence-free form by Edwards et al. (2001). This model, with coefficients optimized using Galileo data, has been employed, for example, in the modeling work by Cowley

©2019. The Authors.

This is an open access article under the terms of the Creative Commons Attribution License, which permits use, distribution and reproduction in any medium, provided the original work is properly cited.

et al. (2008) and Cowley et al. (2017), who incorporated a physical model of the magnetosphere-ionosphere coupling currents leading to the sweepback azimuthal fields in the Jovian system. The Connerney et al. (1981) model has also been successfully modified for the Saturn magnetosphere system and applied to modeling of Pioneer-11, Voyager, and Cassini data (Bunce & Cowley, 2003; Bunce et al., 2007, 2008; Connerney et al., 1983, Giampieri & Dougherty, 2004).

An alternative approach to Jovian magnetodisk modeling was discussed by Goertz (1976a), who introduced the approach of describing the field in terms of Euler potentials. In particular, this method provides an easy way to include the effects of sweepback of the magnetic field lines. Subsequently, Khurana (1997) significantly improved the Goertz (1976a) model by incorporating a model of the current sheet curvature discussed by Khurana (1992), which is due to radial propagation and solar wind effects. A different model of the Jovian magnetosphere that is global in scope was also developed by Alexeev and Belenkaya (2005), which includes the planetary field, shielding currents on a model magnetopause, a magnetotail system, and partially penetrating interplanetary field. This model also includes a sheet current disk in the magnetic equatorial plane, with an azimuthal current intensity that varies as the inverse square of the distance from the planet.

Preliminary study showed by comparison with the presently available Juno data that the paraboloid model of (Alexeev & Belenkaya, 2005), which has been successfully applied to many planetary magnetospheres, gives acceptable but not perfect fitting to the data due to the form of the disc model employed. In this paper we present a new model of Jupiter's current disk, applicable at radial distances between ~ 5 and $\sim 60 R_J$, which incorporates appropriate elements from these previous models, namely, a current density with piecewise variable radial dependency based on the models of Connerney et al. (1981) and Alexeev and Belenkaya (2005), as well as current sheet curvature effects as modeled by Khurana (1997). We find optimal parameters to describe the Juno Perijove-01 data and compare the results with related results from previous models.

2. Connerney et al. (1981) Current Sheet Model

The improved model of the current sheet field developed here starts from the approach of Connerney et al. (1981), which we now briefly consider. We employ cylindrical magnetic equatorial coordinates in which the z axis coincides with the dipole axis of the internal planetary field, and ρ is the perpendicular distance from the axis. The field is axisymmetric with only azimuthal currents, for which the vector potential can be written as

$$\mathbf{A} = A(\rho, z)\mathbf{e}_\phi. \quad (1)$$

Where there are no currents, function A satisfies

$$(\nabla \times \mathbf{B})_\phi = -\frac{\partial^2 A}{\partial z^2} + \frac{A}{\rho^2} - \frac{1}{\rho} \frac{\partial A}{\partial \rho} - \frac{\partial^2 A}{\partial \rho^2} = 0, \quad (2)$$

the general solution for which is

$$A^\pm = \int_0^\infty d\lambda C(\lambda) J_1(\lambda \rho) e^{\mp \lambda z}, \quad (3)$$

where J_1 is a Bessel function of the first order and $C(\lambda)$ is determined from the boundary conditions. The upper sign in equation (3) is for $z > 0$ and the lower for $z < 0$. For a sheet current confined to the plane $z = 0$, the change in radial field across the sheet is given from Ampère's law by

$$\left. \frac{\partial A^+}{\partial z} \right|_{z=0} = \left. \frac{\partial A^-}{\partial z} \right|_{z=0} - \mu_0 I(\rho), \quad (4)$$

where $I(\rho)$ is the surface azimuthal current intensity. Substitution of equation (3) into equation (4) results in

$$\frac{\mu_0 I(\rho)}{2} = \int_0^\infty d\lambda C(\lambda) \lambda J_1(\lambda \rho). \quad (5)$$

Using the Fourier-Bessel equation

$$I(\rho) = \int_0^\infty d\xi \xi I(\xi) \int_0^\infty d\lambda \lambda J_1(\xi \lambda) J_1(\rho \lambda) \quad (6)$$

and equation (5), we find

$$C(\lambda) = \frac{\mu_0}{2} \int_0^\infty d\rho \rho I(\rho) J_1(\rho\lambda). \quad (7)$$

A current with finite thickness can be obtained from the superposition of infinitesimal surface currents, giving

$$A^\pm = \int_0^\infty d\lambda \frac{2C(\lambda)}{\lambda} J_1(\lambda\rho) e^{\mp\lambda z} \sinh(\lambda D), \quad |z| > D, \quad (8)$$

$$A^i = \int_0^\infty d\lambda \frac{2C(\lambda)}{\lambda} J_1(\lambda\rho) [1 - e^{-\lambda D} \cosh(\lambda z)], \quad |z| < D, \quad (9)$$

where D is the half thickness of the current sheet, A^\pm applies to the region outside the current sheet on either side, and A^i applies to the region inside the sheet. The curl of the vector potential gives the following expressions for the field components

$$B_\rho(\rho, z) = \operatorname{sgn}(z) \int_0^\infty d\lambda C(\lambda) J_1(\lambda\rho) e^{-\lambda|z|} \sinh(\lambda D), \quad (10)$$

$$B_z(\rho, z) = \int_0^\infty d\lambda C(\lambda) J_0(\lambda\rho) e^{-\lambda|z|} \sinh(\lambda D), \quad (11)$$

$$B_\rho^i(\rho, z) = \int_0^\infty d\lambda C(\lambda) J_1(\lambda\rho) e^{-\lambda D} \sinh(\lambda z), \quad (12)$$

$$B_z^i(\rho, z) = \int_0^\infty d\lambda C(\lambda) J_0(\lambda\rho) [1 - e^{-\lambda D} \cosh(\lambda z)]. \quad (13)$$

3. Choice of Current Density Function

Connerney et al. (1981) consider a specific choice of $I(\rho)$ given by

$$\begin{aligned} I(\rho) &= 0, \rho \leq a, \\ I(\rho) &= I_0/\rho, \rho > a, \end{aligned} \quad (14)$$

where a is the radial distance of the inner edge of the current sheet disk, which results in an analytical expression for $C(\lambda)$

$$C_1(\lambda) = \frac{\mu_0 I_0}{2} \int_a^\infty d\rho J_1(\rho\lambda) = \frac{\mu_0 I_0}{2\lambda} J_0(\lambda a). \quad (15)$$

As indicated by Connerney et al. (1981), this model applies only to radial distances within $\sim 30 R_J$ of the planet. At larger distances the Connerney et al. (1981) model tends to overestimate the current sheet fields, as shown below in section 5 and Appendix A, such that a model with a faster decrease in current than ρ^{-1} is required. We thus consider the following variant of $I(\rho)$, employed previously in the Alexeev and Belenkaya (2005) model

$$\begin{aligned} I(\rho) &= 0, \rho \leq a, \\ I(\rho) &= I_0 R / \rho^2, \rho > a, \end{aligned} \quad (16)$$

where R is a radial scale length. The expression for $C(\lambda)$ is then

$$C_2(\lambda) = \frac{\mu_0 I_0 R}{2} \int_{a\lambda}^\infty d(\rho\lambda) \frac{J_1(\rho\lambda)}{\rho\lambda}, \quad (17)$$

which can be integrated numerically for various λ and interpolated for use in the integrals in equations (10)–(13).

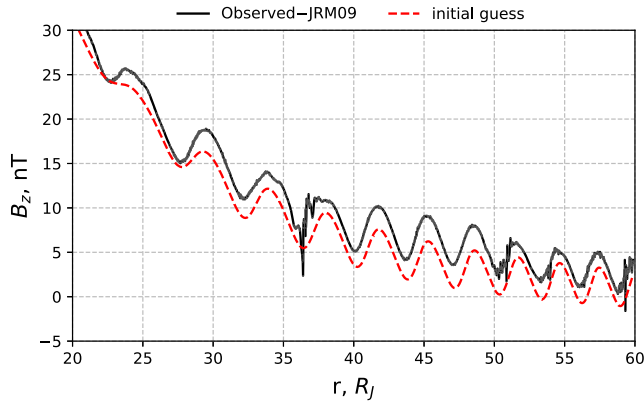


Figure 1. The red line shows the B_z field versus radial distance r from the planet's center calculated from a model with an initially guessed current distribution with current proportional to ρ^{-1} closer to the planet but proportional to ρ^{-2} at larger distances. The data from the Perijove-01 outbound pass are shown. This is compared with the corresponding residual Juno Perijove-01 magnetic field data (black line) from which the JRM09 internal field model of Connerney et al. (2018) has been subtracted. Referring to equation (18) with $R_2 = R_{\text{out}}$, the parameters of the model shown are $I_0 = 26 \times 10^6 \text{ A}/R_J R_{\text{in}} = 7 R_J$, $R_{\text{out}} = 95 R_J$, $R_1 = 27 R_J$.

4. Curvature of the Current Sheet

As discussed previously by Khurana, (1992, 1997), while close to the planet, the current sheet is centered approximately in the planet's magnetic equatorial plane; further away, it deviates from this plane due to the finite radial propagation speed of the effects due to the rotating tilted planetary dipole, combined with the effects of the solar wind flow past the magnetosphere. Khurana (1997) proposed a model of a nonrigid current disk by the variable substitution in the Euler potentials given by

$$z \rightarrow z - z_{\text{cs}}(\rho, \phi), \quad (19)$$

where z_{cs} is the z coordinate of the current sheet center at radial distance ρ and azimuth ϕ in cylindrical magnetic equatorial coordinates. Here we follow a similar procedure but with vector potential \mathbf{A}

$$A^\pm = \int_0^\infty d\lambda \frac{2C(\lambda)}{\lambda} J_1(\lambda\rho) e^{\mp\lambda(z-z_{\text{cs}})} \sinh(\lambda D). \quad (20)$$

$$A^i = \int_0^\infty d\lambda \frac{2C(\lambda)}{\lambda} J_1(\lambda\rho) [1 - e^{-\lambda D} \cosh(\lambda(z - z_{\text{cs}}))]. \quad (21)$$

The curl of these potentials gives us the expressions for the magnetic field of the curved current sheet \mathbf{B}_{curv} , which can be written compactly by using equations (10)–(13) as follows

$$(\mathbf{B}_{\text{curv}})_\rho = B_\rho(\rho, z - z_{\text{cs}}) \quad (22)$$

$$(\mathbf{B}_{\text{curv}})_z = B_z(\rho, z - z_{\text{cs}}) + \frac{\partial z_{\text{cs}}}{\partial \rho} B_\rho(\rho, z - z_{\text{cs}}). \quad (23)$$

These expressions are the same for the regions inside and outside of the current sheet, with appropriate choice of the corresponding fields in

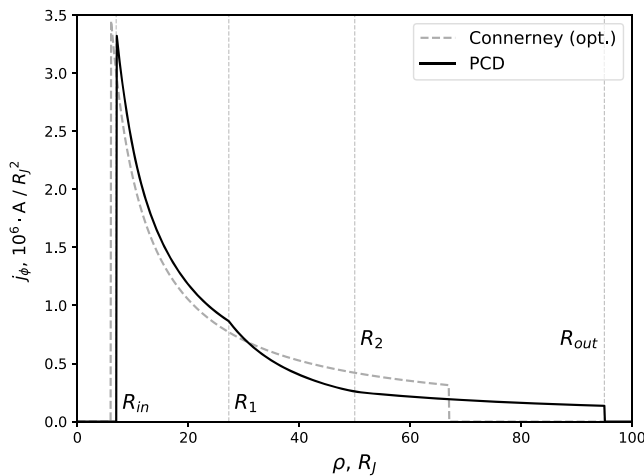


Figure 2. Azimuthal current density as a function of the radial distance. The solid curve is for the PCD model optimized to the Juno Perijove-01 data, while the dashed curve is for a similarly optimized direct Connerney et al. (1981) model. PCD = Piecewise Current Disk.

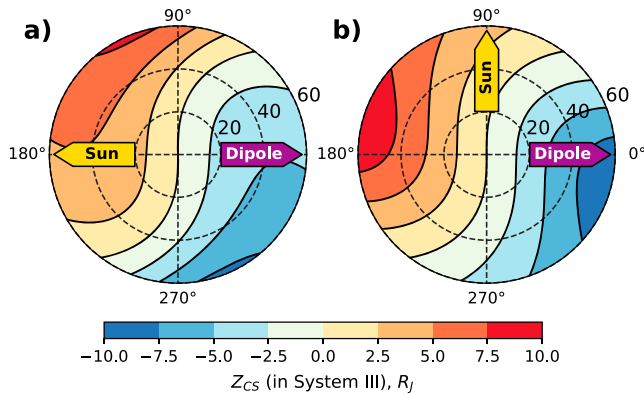


Figure 3. (a, b) Color coded contour plots of the distance of the current sheet center z_{cs} from the jovigraphic equatorial plane given by equations (24) and (25), shown versus System III longitude and radial distance ρ to $60 R_J$ as marked. Black solid lines are lines of constant z_{cs} . Yellow arrows marked “Sun” show projections of the Jupiter-Sun direction on the equator, while purple arrows marked “Dipole” show projections of the planetary dipole axis, with two cases being shown, for antiparallel and perpendicular directions.

equations (10)–(13). Here we use the form of z_{cs} proposed by Khurana, (1992, 1997), in cylindrical magnetic coordinates given by

$$z_{cs} = \rho \tan(\psi_0) \left[\frac{x_0}{x} \tanh(x/x_0) \cos(\phi - \delta) + \cos(\phi) \right], \quad (24)$$

$$\delta(\rho) = \pi - \frac{\Omega_J \rho_0}{v_0} \ln \cosh(\rho/\rho_0). \quad (25)$$

Here x is distance along the Jupiter-Sun axis, ρ and ϕ are cylindrical magnetic coordinates, ψ_0 is the tilt angle of the dipole axis, Ω_J is the angular frequency of Jupiter’s rotation, and x_0 , v_0 , and ρ_0 are the parameters described by Khurana (1992). We note that these expressions were initially constructed for use in the nightside magnetosphere, while Juno Perijove-01 was located in the dawn sector. However, this choice of z_{cs} was found to work well without changing the parameters determined by Khurana (1992). Figure 3 shows contour plots of z_{cs} versus radial distance and azimuth for situations in which the projections of the dipole axis and the Jupiter-Sun direction on the jovigraphic equatorial plane are antiparallel and perpendicular to each other, respectively.

Figure 4 shows the model azimuthal current density in a meridian cross section of the magnetodisk, calculated numerically from curl \mathbf{B} . It can be seen that the resulting current distribution is as intended, that is, a rectangular sheet as in Connerney et al. (1981) but with a slight curvature.

5. Comparison of the PCD Model and Other Models With Juno Perijove-01 Data

The model employed for the internal field of the planet is evidently important when testing current sheet models. Aside from the fact that the internal field is part of the total model field, it also determines the position of the planetary dipole axis and hence the position of the current disk. Here we employ the JRM09 internal field model throughout, constructed by Connerney et al. (2018), using magnetometer data from the first nine orbits of the Juno spacecraft. As illustrated in Figure 5, where we show only model internal fields (no current disk), this model (red line) fits the near-periapsis Juno Perijove-01 data (black line) significantly better than previous models, for example, the VIP4 model of Connerney et al., 1998 (1998; blue dashed line). The JRM09 magnetic field model is a 10 degree model derived from a partial solution to a 20 degree fit to the first nine orbits (Connerney et al., 2018). Terms of higher degree, which are utilized in the fit, covary significantly and thus cannot be uniquely determined until more orbits are available. Inside of the orbit of Io, where the magnetic field magnitude is $\sim 2,000$ nT and growing rapidly with decreasing distance, the magnetodisk represents a small fraction of the observed field; where the field exceeds a few Gauss, the contribution of the magnetodisk is insignificant. Therefore, we consider in this work only observations beyond $5 R_J$ radial distance. In subsequent figures the region inside $5 R_J$ is marked by a gray bar where the current sheet field is “not distinguishable” as labelled.

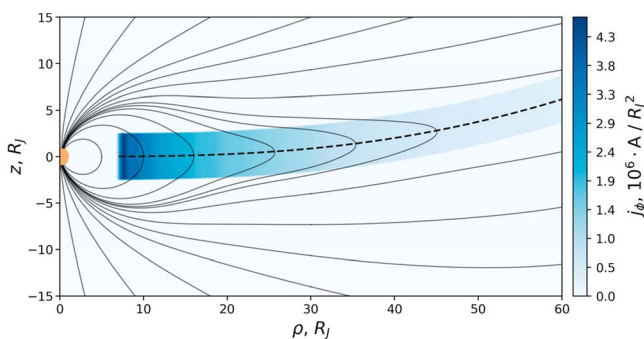


Figure 4. Cross section of the model current sheet in the $\phi = \frac{\pi}{4}$ meridian plane, showing color coded azimuthal current density for the PCD model, calculated from curl \mathbf{B} . The solid lines show the field lines of the PCD model combined with the JRM09 internal field of Connerney et al. (2018). The dashed line shows the current sheet center. PCD = Piecewise Current Disk.

Here as well as the PCD model, we tested several other empirical models of the Jovian current disk. For PCD model we used parameter values listed in Table 1 (see equation (18)), which were determined by minimizing the root-mean-square (RMS) deviation of the modeled field from that observed on Juno Perijove-01. It should be noted, however, that not all of the parameters are tightly constrained, such that some of them could be altered without significant change in the RMS error. Also, as indicated above, the parameters of the current sheet curvature were taken from Khurana (1997) without further modification. With this set of parameters the total current in the Perijove-01 PCD model is about 250 MA, which is in approximate accord with previous values (e.g., Connerney et al., 1981). For the Connerney et al. (1981) model direct, we

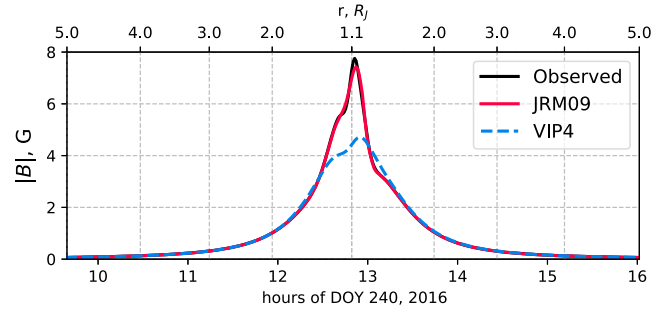


Figure 5. Comparison between the strength of the observed field on Juno Perijove-01 (black line) and the calculated fields using the VIP4 model of Connerney et al., 1998 (1998; blue dashed line) and the JRM09 model of Connerney et al., 1981 (1981; red line). No current disk field is included. $1 \text{ G} = 10^5 \text{ nT}$.

also optimized the parameters to fit the Juno Perijove-01 data, though keeping half width D fixed at $2.5 R_J$, finding $I_0 = 21 \times 10^6 \text{ AR}_J^{-1}$ (equivalent to $\mu_0 I_0 / 2 \approx 185 \text{ nT}$), $R_0 = 6 R_J$, and $R_1 = 67 R_J$. We note that these parameters (employed in Figure 2) are close to those used previously in the modeling work by Cowley et al., 2008 (2008, 2017). The parameters originally determined by Connerney et al. (1981) from fits to Pioneer-10 and Voyager-1 data were $I_0 \approx 25.6 \times 10^6 \text{ AR}_J^{-1}$ ($\mu_0 I_0 / 2 = 225 \text{ nT}$), $R_0 = 5 R_J$, and $R_1 = 50 R_J$, with the current parameter being modified to $I_0 \approx 17.1 \times 10^6 \text{ AR}_J^{-1}$ (equivalent to $\mu_0 I_0 / 2 = 150 \text{ nT}$) for Voyager-2 data. A subsequent combined fit of the internal planetary field plus current sheet field to the Voyager-1 data also yielded a smaller current parameter of $I_0 = 21 \times 10^6 \text{ AR}_J^{-1}$ together with $R_0 = 5 R_J$ and $R_1 = 50 R_J$ (Connerney et al., 1982). The magnetodisk parameters used in the Alexeev and Belenkaya (2005) magnetospheric model are inner and outer radii of the disk (R_{DC1} and R_{DC2}) and magnetodisk field at the outer boundary (B_{DC}), with values optimized for the inbound Ulysses pass of $R_{DC1} = 95 R_J$, $R_{DC2} = 18.4 R_J$, and $B_{DC} = 2.5 \text{ nT}$. The values optimized for Juno Perijove-01 employed here (with other less important parameters held fixed) are $R_{DC1} = 95 R_J$, $R_{DC2} = 9 R_J$, and $B_{DC} = 2.2 \text{ nT}$. The Khurana (1997) model was constructed using data from the Pioneer-10, Voyager-1, and Voyager-2 flybys. The model has 14 parameters that we were not able to determine properly from the fit to the Juno data, so that comparison of the model with these data is not fully valid. Thus, we additionally compared the model with the PCD fit to the Pioneer-10 outbound data, using the following parameters for the PCD: $I_0 = 21 \times 10^6 \text{ A/R}_J$, $D = 2.5 R_J$, $R_{in} = 7 R_J$, $R_{out} = 80 R_J$, $R_1 = 30 R_J$, $R_2 = 40 R_J$.

In Figure 6 we compare the results of the PCD model with the residual poloidal components observed by the Juno spacecraft on Perijove-01 (1-min averages), from which the JRM09 internal field has been subtracted. The fields are plotted versus radial distance r from the planet's center, with the data from the inbound trajectory on the left of the origin and the data from the outbound trajectory on the right. For quantitative comparison of the goodness of fit we used the RMS deviation of the predicted field from the observed field but excluding B_ϕ , that is,

$$S = \sqrt{\frac{1}{n} \sum_{k=1}^n (B_\rho^k - \Delta B_\rho^k)^2 + (B_z^k - \Delta B_z^k)^2}, \quad (26)$$

where n is the number of data points, $B_{\rho,z}$ are the field components derived from the current sheet model, and $\Delta B_{\rho,z}$ are the observed residual fields following subtraction of the JRM09 internal field model from the observations. Among the models considered here only that of Khurana (1997) includes an azimuthal component, which we do not consider here so that all of the comparisons are made on a similar basis. For a more detailed comparison we also divide the trajectory in three radial regions, namely, the inner region with radial distances between 5 and $15 R_J$, the middle region between 15 and $40 R_J$, and the outer region between 40 and $60 R_J$. We do not consider the region beyond $60 R_J$ because the influence of the currents on

Table 1
PCD Model Parameters Fitted to Juno Perijove-01 Magnetic Field Data

I_0	D	R_{in}	R_{out}	R_1	R_2
$26.3 \times 10^6 \text{ A/R}_J$	$2.5 R_J$	$7.1 R_J$	$95 R_J$	$27.3 R_J$	$50 R_J$

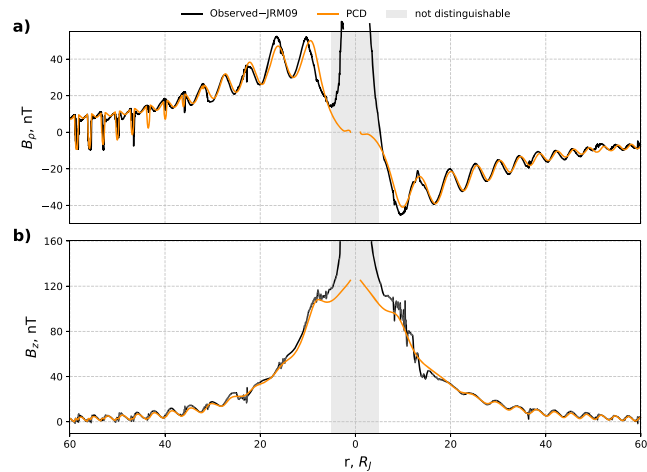


Figure 6. Comparison of the poloidal fields calculated from the PCD model (orange line) and the observed residual field on Juno Perijove-01 from which the JRM09 internal field has been subtracted (black line). (a, b) The cylindrical ρ and z field components, respectively. The fields are plotted versus radial distance r from the planet’s center with data from the inbound and outbound trajectories being shown to the left and right of the origin, respectively. The part of the trajectory where the field of the current disk becomes indistinguishable on the background of the internal field is marked by the gray band as “not distinguishable”. PCD = Piecewise Current Disk.

the magnetopause and tail then becomes significant. We also do not consider the region closer than $5 R_J$ for the reasons outlined above.

Figure 7 shows the RMS errors for all the above models in each of the three radial regions, while the detailed fits for the other models are shown in Figures A1 –A3 in Appendix A. In the inner region the model by Khurana (1997) has large error compared with the PCD, Alexeev and Belenkaya (2005) and the optimized Connerney et al. (1981) model, with the Khurana (1997) model being offscale at ~ 190 nT. In the middle region, the Khurana (1997) model starts to work better (note also the change in plot scale), with the Alexeev and Belenkaya (2005) model having the largest error, the PCD model the smallest error, and the optimized Connerney et al. (1981) model being intermediate. We also note that in both the inner and middle regions, the “curved” and “not curved” versions of the PCD model show very similar results, due to the small deviation of the current disk from the magnetic equator at these distances. In the outer region in Figure 7, however, the picture is rather different, with the curved PCD and Khurana (1997) models showing similar

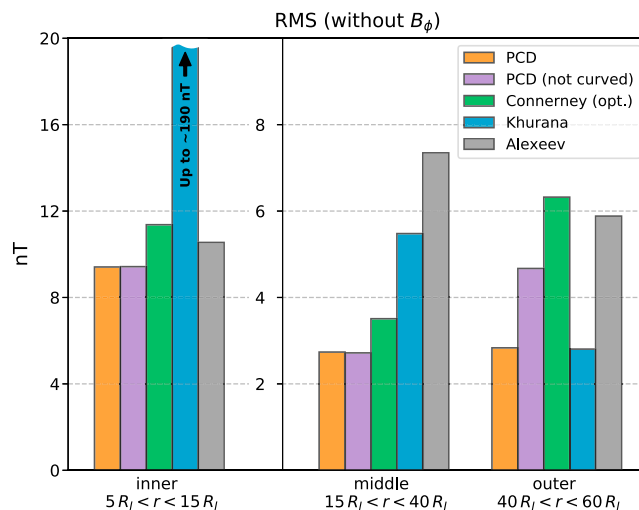


Figure 7. RMS error of the models in the inner, middle, and outer regions of the Juno Perijove-01 trajectory. PCD = Piecewise Current Disk; RMS = root-mean-square.

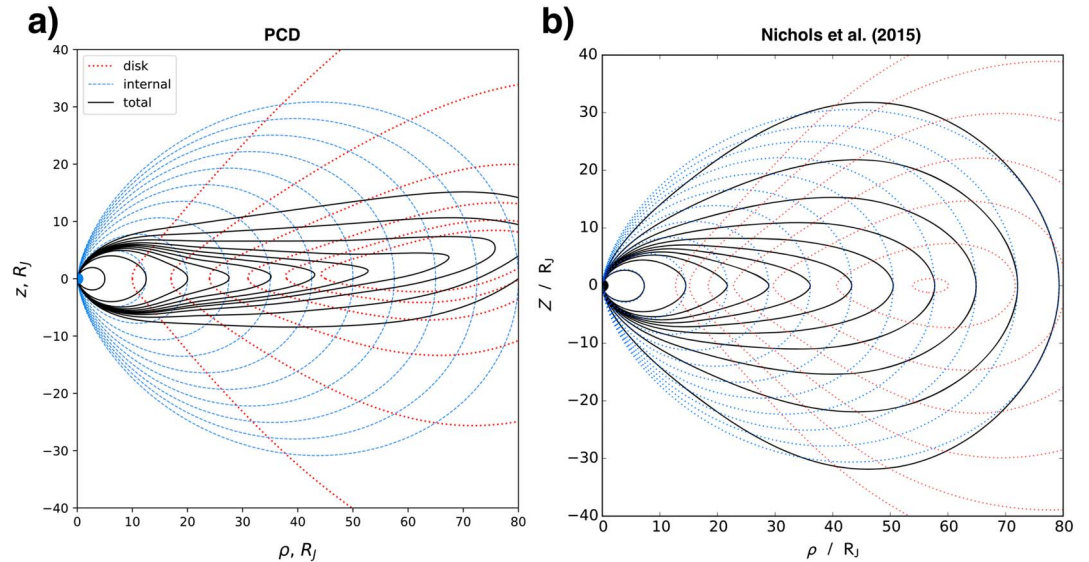


Figure 8. (a) Field lines of the PCD model current disc (red lines), the JRM09 internal planetary field (blue lines), and the combined field (black lines). (b) Reproduced Figure 5 of Nichols et al. (2015), showing field lines of the self-consistent physical model current sheet (red lines), the planetary dipole field (blue lines), and the combined field (black lines). PCD = Piecewise Current Disk.

best fits, while the optimized Connerney et al. (1981) and Alexeev and Belenkaya (2005) models have similar larger errors. We note that the Connerney et al. (1981) model, as originally published, was limited to the radial range $r < 30R_J$ and was not intended to describe the more distant magnetodisk. At those distances the effects of the current sheet curvature become significant, as shown in Figure A4 in Appendix A.

Figure A5 shows results for the comparison of the Khurana (1997) model and the PCD model for the Pioneer-10 outbound data. Similar to the case of the Juno Perijove-01 data, in the inner magnetosphere the Khurana model gives a very large error in comparison with the PCD model. In the middle magnetosphere, both models demonstrate similar errors, while in the outer magnetosphere the Khurana model has a significantly lower error in comparison with the PCD model.

In Figure 8 we compare the general structure of the field in the Nichols et al. (2015) self-consistent model with the PCD empirical model. The field lines of the planetary internal field are shown by the blue lines; those of the current sheet alone are shown by the red lines, while the combined fields are shown by the black lines. Both models give a similar field structure in the inner part of the system closer than $30R_J$ but differ significantly further away, where the PCD model displays more radially stretched field lines than the Nichols et al. (2015) model, indicative of larger current densities. Of course, the structure of the field in the outer magnetosphere is significantly variable, depending on the LT of observation, as well as on the dynamic pressure of the solar wind, particularly in the dayside sector.

6. Conclusions

We have described a new empirical model of the Jovian current sheet or magnetodisk, constructed on the basis of previous models introduced by Connerney et al. (1981), Alexeev and Belenkaya (2005), and Khurana (1997). It employs a piecewise dependence of the current density on distance ρ from the dipole axis of Jupiter, chosen to be proportional to ρ^{-1} at inner distances between ~ 7 and $\sim 30R_J$ and again at distances between ~ 50 and $\sim 95R_J$ but to be continuous in value and proportional to ρ^{-2} at distances between. For this reason we term the model the PCD model. It also takes into account the curvature of the magnetodisk with distance and azimuth using the approach given by Khurana (1997). The model is taken to be applicable in the radial distance range between 5 and $\sim 60R_J$. The model has been compared with Juno magnetometer data obtained on Perijove-01, with detailed best fit model parameters being determined. Compared with previous models similarly optimized, the PCD model shows the lowest RMS deviation.

Appendix A: Additional Figures

In Figures A1, A2, and A3 we compare results of the PCD model as shown in Figure 6 with those using the optimized Connerney et al. (1981), Alexeev and Belenkaya (2005), and Khurana (1997) models, respectively, using the same figure format.

The difference between the fields generated by the rigid and curved versions of the PCD model in the outer inbound region is shown for the B_ρ and B_z components in Figures A4a and A4b, respectively.

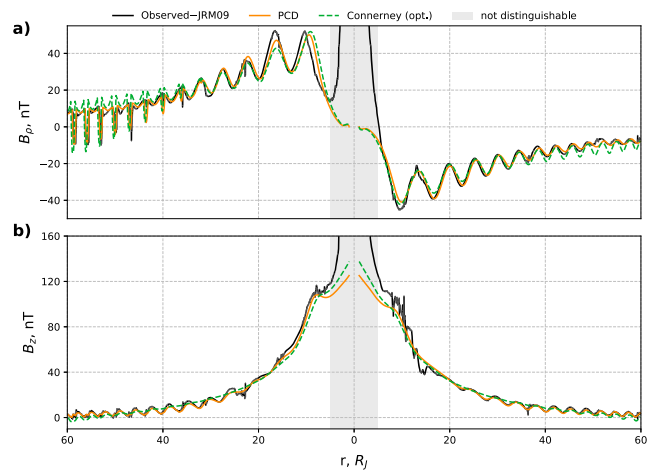


Figure A1. As in Figure 6 but with results from the optimized Connerney et al. (1981) model added (green dashed line).

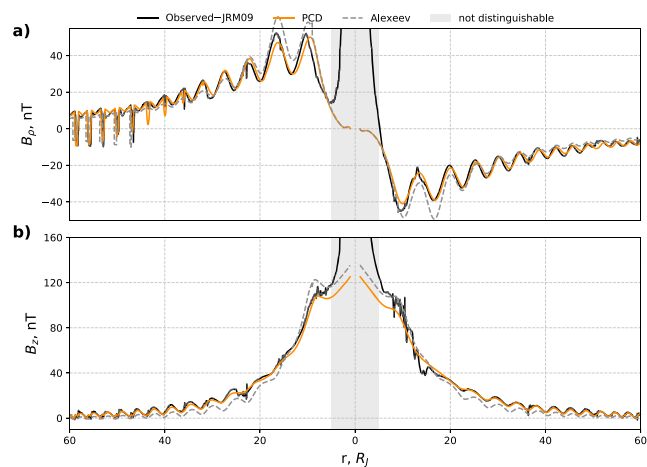


Figure A2. As in Figure 6 but with results from the Alexeev and Belenkaya (2005) model added (gray dashed line).

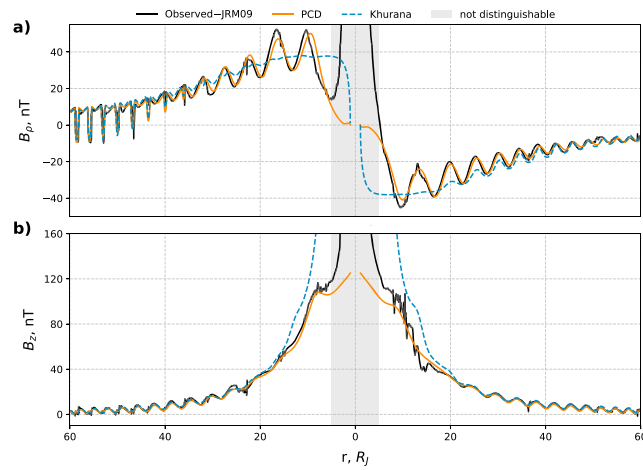


Figure A3. As in Figure 6 but with results from the Khurana (1997) model added (blue dashed line).

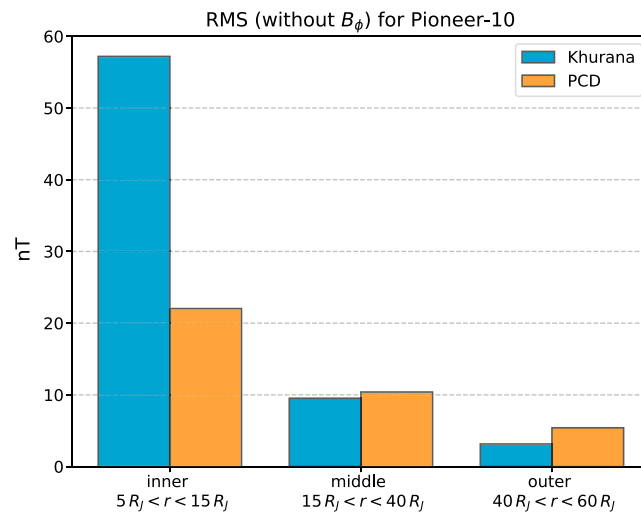


Figure A4. Comparison between the rigid (purple dashed line) and curved (orange line) PCD model results in the outer inbound region of the Juno Perijove-01 trajectory. Figures A4a and A4b show the cylindrical ρ and z field components, respectively.

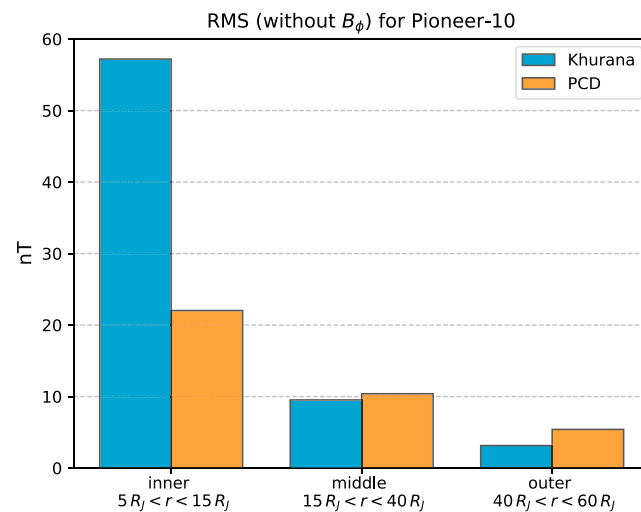


Figure A5. RMS error of the PCD model and the Khurana (1997) model in the inner, middle, and outer regions of the Pioneer-10 outbound pass. RMS = root-mean-square; PCD = Piecewise Current Disk.

Acknowledgments

Work at the Federal State Budget Educational Institution of Higher Education M.V. Lomonosov Moscow State University, Skobel'syn Institute of Nuclear Physics (SINP MSU), was partially supported by the Ministry of Education and Science of the Russian Federation (grant RFMEFI61617X0084). Work at the University of Leicester was supported by STFC Consolidated Grant ST/N000749/1. The Juno magnetometer data were obtained from the Planetary Data System (PDS; <https://pds-ppi.igpp.ucla.edu>). We are grateful to the Juno team for making the magnetic field data available (FGM instrument scientist J. E. P. Connerney; principal investigator of Juno mission Scott J. Bolton). Source code for the PCD model is available at the website (<https://github.com/gasgiant/jfield>). Email author (pensionerov@gmail.com) if you have any questions.

References

- Acuña, M. H., Behannon, K. W., & Connerney, J. E. P. (1983). Jupiter's magnetic field and magnetosphere. In A. J. Dessler (Ed.), *Physics of the Jovian magnetosphere* (pp. 1–50). Cambridge and New York: Cambridge University Press. <https://doi.org/10.1017/cbo9780511564574.003>
- Alexeev, I. I., & Belenkaya, E. S. (2005). Modeling of the Jovian magnetosphere. *Annales Geophysicae*, 23(3), 809–826. <https://doi.org/10.5194/angeo-23-809-2005>
- Bagenal, F. (2007). The magnetosphere of Jupiter: Coupling the equator to the poles. *Journal of Atmospheric and Solar-Terrestrial Physics*, 69(3), 387–402. <https://doi.org/10.1016/j.jastp.2006.08.012>
- Balogh, A., Beekand, T. J., Forsyth, R. J., Hedgecock, P. C., Marquedant, R. J., Smith, E. J., & Tsurutani, B. T. (1992). The magnetic field investigation on the Ulysses mission—Instrumentation and preliminary scientific results. *Astronomy and Astrophysics Supplement Series*, 92(2), 221–236.
- Balogh, A., Dougherty, M. K., Forsyth, R. J., Southwood, D. J., Smith, E. J., Tsurutani, B. T., & Burton, M. E. (1992). Magnetic field observations during the Ulysses Flyby of Jupiter. *Science*, 257(5076), 1515–1518. <https://doi.org/10.1126/science.257.5076.1515>
- Bolton, S. J., Bagenal, F., Blanc, M., Cassidy, T., Chané, E., Jackman, C., & Waite, H. (2015). Jupiter's magnetosphere: Plasma sources and transport. *Space Science Reviews*, 192(1–4), 209–236. <https://doi.org/10.1007/s11214-015-0184-5>
- Bunce, E. J., Arridge, C. S., Cowley, S. W. H., & Dougherty, M. K. (2008). Magnetic field structure of Saturn's dayside magnetosphere and its mapping to the ionosphere: Results from ring current modeling. *Journal of Geophysical Research*, 113, A02207. <https://doi.org/10.1029/2007JA012538>
- Bunce, E. J., & Cowley, S. W. H. (2003). A note on the ring current in Saturn's magnetosphere: Comparison of magnetic data obtained during the Pioneer-11 and Voyager-1 and -2 flybys. *Annales Geophysicae*, 21(3), 661–669. <https://doi.org/10.5194/angeo-21-661-2003>
- Bunce, E. J., Cowley, S. W. H., Alexeev, I. I., Arridge, C. S., Dougherty, M. K., Nichols, J. D., & Russell, C. T. (2007). Cassini observations of the variation of Saturn's ring current parameters with system size. *Journal of Geophysical Research*, 112, A10. <https://doi.org/10.1029/2007JA012275>
- Caudal, G. (1986). A self-consistent model of Jupiter's magnetodisc including the effects of centrifugal force and pressure. *Journal of Geophysical Research*, 91(A4), 4201. <https://doi.org/10.1029/JA091ia04p04201>
- Connerney, J. E. P., Acuña, M. H., & Ness, N. F. (1981). Modeling the Jovian current sheet and inner magnetosphere. *Journal of Geophysical Research*, 86(A10), 8370–8384. <https://doi.org/10.1029/JA086ia10p08370>
- Connerney, J. E. P., Acuña, M. H., & Ness, N. F. (1982). Voyager 1 assessment of Jupiter's planetary magnetic field. *Journal of Geophysical Research*, 87(A5), 3623. <https://doi.org/10.1029/JA087ia05p03623>
- Connerney, J. E. P., Acuña, M. H., & Ness, N. F. (1983). Currents in Saturn's magnetosphere. *Journal of Geophysical Research*, 88(A11), 8779–8789. <https://doi.org/10.1029/JA088ia11p08779>
- Connerney, J. E. P., Acuña, M. H., Ness, N. F., & Satoh, T. (1998). New models of Jupiter's magnetic field constrained by the Io flux tube footprint. *Journal of Geophysical Research*, 103(A6), 11,929–11,939. <https://doi.org/10.1029/97JA03726>
- Connerney, J. E. P., Kotsiaros, S., Oliverson, R. J., Espley, J. R., Joergensen, J. L., Joergensen, P. S., & Levin, S. M. (2018). A new model of Jupiter's magnetic field from Juno's First Nine Orbits. *Geophysical Research Letters*, 45, 2590–2596. <https://doi.org/10.1002/2018gl077312>
- Cowley, S. W. H., Deason, A. J., & Bunce, E. J. (2008). Axi-symmetric models of auroral current systems in Jupiter's magnetosphere with predictions for the Juno mission. *Annales Geophysicae*, 26(12), 4051–4074. <https://doi.org/10.5194/angeo-26-4051-2008>
- Cowley, S. W. H., Provan, G., Bunce, E. J., & Nichols, J. D. (2017). Magnetosphere-ionosphere coupling at Jupiter: Expectations for Juno Perijove 1 from a steady state axisymmetric physical model. *Geophysical Research Letters*, 44, 4497–4505. <https://doi.org/10.1002/2017gl073129>
- Edwards, T., Bunce, E., & Cowley, S. (2001). A note on the vector potential of Connerney et al.'s model of the equatorial current sheet in Jupiter's magnetosphere. *Planetary and Space Science*, 49(10–11), 1115–1123. [https://doi.org/10.1016/s0032-0633\(00\)00164-1](https://doi.org/10.1016/s0032-0633(00)00164-1)
- Giamperi, G., & Dougherty, M. K. (2004). Modelling of the ring current in Saturn's magnetosphere. *Annales Geophysicae*, 22(2), 653–659. <https://doi.org/10.5194/angeo-22-653-2004>
- Goertz, C. K. (1976a). The current sheet in Jupiter's magnetosphere. *Journal of Geophysical Research*, 81(19), 3368–3372. <https://doi.org/10.1029/JA081i019p03368>
- Goertz, C. K. (1976b). Jupiter's magnetosphere—Particles and fields. In T. Gehrels & S. Matthews (Eds.), *IAU Colloq. 30: Jupiter: Studies of the interior, atmosphere, magnetosphere and satellites* (pp. 32–58). Tucson: University of Arizona Press.
- Goertz, C. K., & Ip, W. H. (1984). A dawn-to-dusk electric field in the Jovian magnetosphere. *Planetary and Space Science*, 32(2), 179–185. [https://doi.org/10.1016/0032-0633\(84\)90152-1](https://doi.org/10.1016/0032-0633(84)90152-1)
- Hill, T. (1979). Inertial limit on corotation. *Journal of Geophysical Research*, 84(A11), 6554. <https://doi.org/10.1029/JA084ia11p06554>
- Joy, S. P. (2002). Probabilistic models of the Jovian magnetopause and bow shock locations. *Journal of Geophysical Research*, 107, A10. <https://doi.org/10.1029/2001JA009146>
- Khurana, K. K. (1992). A generalized hinged-magnetodisc model of Jupiter's nightside current sheet. *Journal of Geophysical Research*, 97(A5), 6269. <https://doi.org/10.1029/92JA00169>
- Khurana, K. K. (1997). Euler potential models of Jupiter's magnetospheric field. *Journal of Geophysical Research*, 102(A6), 11,295–11,306. <https://doi.org/10.1029/97JA00563>
- Ness, N. F., Acuna, M. H., Lepping, R. P., Behannon, K. W., Burlaga, L. F., & Neubauer, F. M. (1979). Jupiter's magnetic tail. *Nature*, 280(5725), 799–802. <https://doi.org/10.1038/280799a0>
- Ness, N. F., Acuna, M. H., Lepping, R. P., Burlaga, L. F., Behannon, K. W., & Neubauer, F. M. (1979). Magnetic field studies at Jupiter by Voyager 1: Preliminary results. *Science*, 204(4396), 982–987. <https://doi.org/10.1126/science.204.4396.982>
- Ness, N. F., Acuna, M. H., Lepping, R. P., Burlaga, L. F., Behannon, K. W., & Neubauer, F. M. (1979). Magnetic field studies at Jupiter by Voyager 2: Preliminary results. *Science*, 206(4421), 966–972. <https://doi.org/10.1126/science.206.4421.966>
- Nichols, J. D. (2011). Magnetosphere-ionosphere coupling in Jupiter's middle magnetosphere: Computations including a self-consistent current sheet magnetic field model. *Journal of Geophysical Research*, 116, A10. <https://doi.org/10.1029/2011JA016922>
- Nichols, J. D., Achilleos, N., & Cowley, S. W. H. (2015). A model of force balance in Jupiter's magnetodisc including hot plasma pressure anisotropy. *Journal of Geophysical Research: Space Physics*, 120, 10,185–10,206. <https://doi.org/10.1002/2015ja021807>
- Smith, E., Connor, B., & Foster, G. (1975). Measuring the magnetic fields of Jupiter and the outer solar system. *IEEE Transactions on Magnetics*, 11(4), 962–980. <https://doi.org/10.1109/tmag.1975.1058779>
- Smith, E. J., Davis, L. J., & Jones, D. E. (1976). Jupiter's magnetic field and magnetosphere. In T. Gehrels (Ed.), *Jupiter* (pp. 788). Tucson: University of Arizona Press.

- Smith, E. J., Davis, L., Jones, D. E., Coleman, P. J., Colburn, D. S., Dyal, P., & Frandsen, A. M. A. (1974). The planetary magnetic field and magnetosphere of Jupiter: Pioneer 10. *Journal of Geophysical Research*, *79*(25), 3501–3513. <https://doi.org/10.1029/JA079i025p03501>
- Smith, E. J., Davis, L., Jones, D. E., Coleman, P. J., Colburn, D. S., Dyal, P., & Sonett, C. P. (1975). Jupiter's magnetic field. Magnetosphere, and interaction with the solar wind: Pioneer 11. *Science*, *188*(4187), 451–455. <https://doi.org/10.1126/science.188.4187.451>
- Vasyliunas, V. M. (1983). Plasma distribution and flow. In A. J. Dessler (Ed.), *Physics of the Jovian Magnetosphere* (pp. 395–453). Cambridge: Cambridge University Press.